QUASI-ELLIPTIC BANDPASS FILTER BASED ON SIR WITH ELIMINATION OF FIRST SPURIOUS RESPONSE

N. Molaei Garmjani and N. Komjani

Electrical Engineering Department
Iran University of Science & Technology (IUST)
Narmak, Tehran, Iran

Abstract—In this paper, a quasi-elliptic bandpass filter was designed, simulated, and fabricated using four-pole cross-coupled stepped impedance resonators (SIR). Using a special type of stepped impedance resonators, a great increase in rejection band width of the filter was obtained. In order to perform the mentioned design practically, we utilized a compound sandwich model of two substrates (in strip line form). Furthermore, we used Defected Ground Structure (DGS) in order to omit the first spurious resonant frequency and increase bandwidth of the filter. The fabricated sample was measured, and the results showed a good agreement with simulated results.

1. INTRODUCTION

Nowadays, bandpass filters with high selectiveness and low internal losses in pass band width are required in most of the communication applications, especially mobile systems. For this reason, stepped impedance resonators are extensively used in operative circuits. For having smaller dimensions and higher quality factor, these resonators are used in circuits like duplexers and mixers.

In order to obtain higher selectiveness, poles degree of the filter and consequently the quantity of resonators must be increased. On the other hand, internal losses increase because resonators are not ideal. In this paper, in the design process of SIR filter, we have used four-pole cross-coupled resonators (reciprocal coupling between nonadjacent resonators) in order to obtain high selectiveness. This affair led to more internal losses in the designed filter. Therefore, we utilized the sandwich model idea to decrease the insertion loss.

Corresponding author: N. Molaei Garmjani (nima_molaei@yahoo.com).

Moreover, we eliminated the first spurious resonant frequency with the use of etching defects in the ground plane of the structure.

2. THE BASIC STRUCTURE OF SIR RESONATOR

The basic structure of tri-section SIR resonator is shown in Fig. 1(a). The folded SIR resonator, which is used in our design, is also shown in Fig. 1(c). These resonators not only have smaller dimensions but also own wider rejection bandwidth comparing with other popular resonators.

At first, let us consider a capacitively loaded lossless transmission line resonator of Fig. 1(b). C_L, Z_a, β_a, and d represent the loaded capacitance, the characteristic impedance, the propagation constant, and the length of the unloaded line, respectively. Thus, the electric length is $\theta_a = \beta_a d$. The circuit response of Fig. 1(b) is described by [1]:

$$\begin{bmatrix} V_1 \\ I_1 \end{bmatrix} = \begin{bmatrix} A & B \\ C & D \end{bmatrix} \cdot \begin{bmatrix} V_2 \\ -I_2 \end{bmatrix} \tag{1}$$

where,

$$A = D = \cos\theta_a - \frac{1}{2}\omega C_L Z_a \sin\theta_a \tag{2a}$$

$$B = jZ_a \sin\theta_a \tag{2b}$$

$$C = j\left(\omega C_L \cos\theta_a + \frac{1}{Z_a}\sin\theta_a - \frac{1}{4}\omega^2 C_L^2 Z_a \sin\theta_a\right) \tag{2c}$$

(a)

(b)   (c)
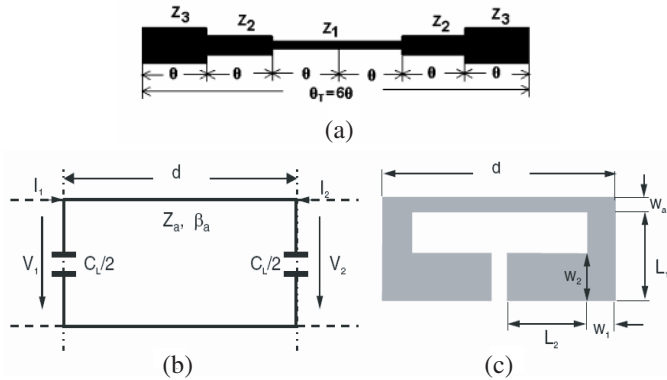
Figure 1. (a) Basic structure of tri-section SIR resonator. (b) An equivalent circuit of proposed SIR resonator. (c) Proposed folded SIR resonator.

And $\omega = 2\pi f$ is the angular frequency; A, B, C, and D are the network parameters of transmission matrix. To fulfill the reciprocal condition and boundary condition, we have:

$$AD - BC = 1$$

By satisfying boundary conditions for the standing wave, we have:

$$I_1 = I_2 = 0$$

$$\frac{C}{A} = \left. \frac{I_1}{V_1} \right|_{I_2=0} = \left. \frac{I_2}{V_2} \right|_{I_1=0} = 0 \tag{3}$$

Because:

$$A = \left. \frac{V_1}{V_2} \right|_{I_2=0} = \begin{cases} -1 & \text{for the main resonant frequency} \\ 1 & \text{for the spurious resonant frequency} \end{cases} \tag{4}$$

From (2a) we have:

$$\begin{cases} \cos\theta_{a0} - \dfrac{1}{2}\omega_0 C_L Z_a \sin\theta_{a0} = -1 & \text{(5a)} \\[2mm] \cos\theta_{a1} - \dfrac{1}{2}\omega_1 C_L Z_a \sin\theta_{a1} = 1 & \text{(5b)} \end{cases}$$

By substituting (5a) and (5b) in (2c) and letting $C = 0$ in (3) we have:

$$\begin{cases} \theta_{a0} = 2\tan^{-1}\left(\dfrac{1}{\pi f_0 Z_a C_L}\right) & \text{(6a)} \\[2mm] \theta_{a1} = 2\pi - 2\tan^{-1}\left(\pi f_1 Z_a C_L\right) & \text{(6b)} \end{cases}$$

The fundamental resonant frequency and the first spurious resonant frequency are f_0 and f_1, respectively. If C_L equals to zero in above equation, then θ_{a0} and θ_{a1} equals to π and 2π, respectively. If $C_L \neq 0$, the resonant frequencies shift down as the loaded capacitance increases.

Here, we have assumed $Z_a = 50\,\Omega$, $d = 12.5\,\text{mm}$, and $W_a = 0.5\,\text{mm}$.

The basic resonator in Fig. 1(c) is used as a unit cell of a periodically loaded transmission line. The function defined in a bounded region is expanded into a periodic function. Substituting Floquet's theorem, i.e.:

$$\begin{cases} V_2 = e^{-j\beta d}V_1 & \text{(7a)} \\[2mm] -I_2 = e^{-j\beta d}I_1 & \text{(7b)} \end{cases}$$

To (1), we have:

$$\begin{bmatrix} A - e^{j\beta d} & B \\ C & D - e^{j\beta d} \end{bmatrix} \begin{bmatrix} V_2 \\ -I_2 \end{bmatrix} = \begin{bmatrix} 0 \\ 0 \end{bmatrix} \tag{8}$$

There is a nontrivial solution for V_2 and I_2 only if the above determinant vanishes. So,

$$\left(A - e^{j\beta d}\right)\left(D - e^{j\beta d}\right) - BC = 0 \tag{9}$$

Equation (9) transforms to the following equation in the symmetry and reciprocal case.

$$\cos\left(\beta d\right) = \cos\theta_a - \frac{1}{2}\omega C_L Z_a \sin\theta_a \tag{10}$$

Therefore, $\cos\left(\beta_0 d\right)$ equals to -1 for the fundamental resonant frequency and $\cos\left(\beta_1 d\right)$ equals to 1 for the first spurious resonant frequency, where:

$$\beta_1 = \frac{\omega_1}{V_{P1}} \text{ and } \beta_0 = \frac{\omega_0}{V_{P0}}$$

In above equations, V_{P0} and V_{P1} are the phase velocities of the loaded line at the fundamental and the first spurious resonant frequencies, respectively. Consequently, we obtain:

$$\frac{f_1}{f_0} = 2\frac{V_{P1}}{V_{P0}} \tag{11}$$
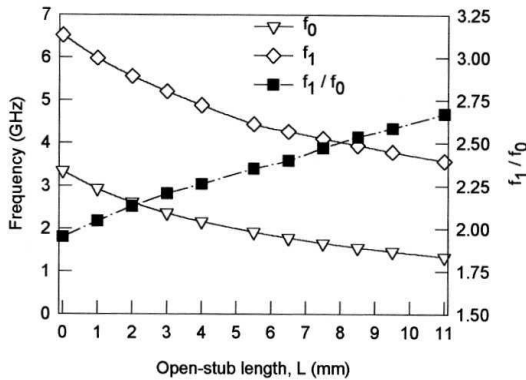
Figure 2. The fundamental, spurious resonant frequencies, and their ratio versus the length of the folded open-stubs [1].

Here, resonator of Fig. 1(c), which is composed of a microstrip line with both ends loaded with folded open-stubs, is used. The folded arms of open-stubs are applied for increasing the loading capacitance to ground for the purpose of cross couplings. Fig. 2 shows the fundamental and spurious resonant frequencies together with their ratio versus the length of folded open-stubs. The length of folded open-stubs (L) is obtained from [1]:

$$\begin{cases} L = L_1 & \text{for } L \le 5.5\,\text{mm} \\ L = 5.5 + L_2 & \text{for } L > 5.5\,\text{mm} \end{cases} \tag{12}$$

The other parameters of folded SIR in Fig. 1(c) have been chosen by simulation and optimization in Section 5, where design of the final filter is performed.

3. FOUR-POLE CROSS-COUPLED SIR FILTER

In order to achieve high selectiveness, the order of filter must increase for the butterworth and Chebyschev filters. Elliptic filter has ripple in the both pass band and rejection band due to having limited transmission zeroes; as a result, it is highly selective and its slope is much more than two above filters. However, the realization of
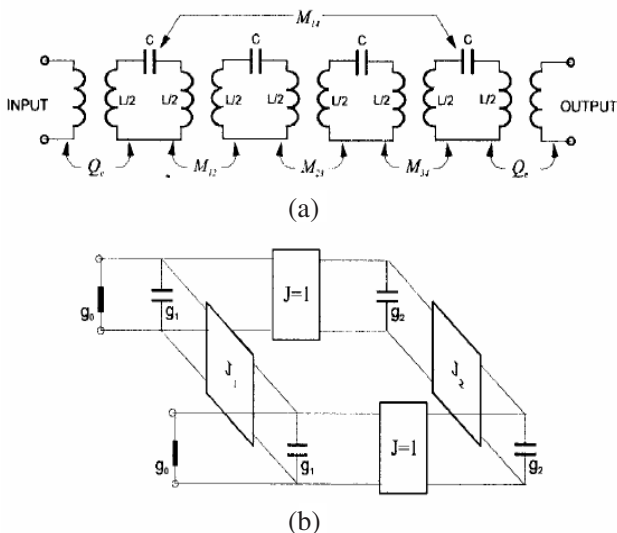
Figure 3. (a) The equivalent circuit of the designed filter. (b) The associated low-pass prototype filter.

this type of filter with the printed circuits structure is complicated. The four-pole cross-coupled SIR filter is designed using the proposed basic resonator structure in Section 2 based on the defined method in [2]. Fig. 3(a) shows the equivalent circuit of the designed filter, in which M_{14} represents the mixed coupling between input and output resonators. This pass band filter can be associated with the low-pass prototype filter of Fig. 3(b), that the values of elements are computable by described approaches in [2]. External quality factor Q_e and filter coupling coefficients are determined from [1]:

$$
\begin{aligned}
Q_e &= \frac{g_0 g_1}{FBW} & M_{23} &= \frac{FBW \cdot J_2}{g_2} \\
M_{12} = M_{34} &= \frac{FBW}{\sqrt{g_1 g_2}} & M_{14} &= \frac{FBW \cdot J_1}{g_1}
\end{aligned}
\tag{13}
$$

More details about electric, magnetic, and mixed coupling between the resonators are discussed in [4].

The sandwich model schematic of four-pole SIR filter is shown in Fig. 4.
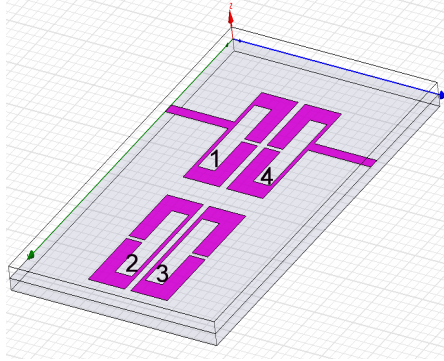
Figure 4. The sandwich model schematic of four-pole SIR filter.

4. SIR FILTER WITH DGS STRUCTURE IN ITS GROUND PLANE

One method to improve the filter characteristics is to use microstrip structures with defected ground plane. DGS cells are used as complementary of the main filter and also independently in executing the filter, due to having natural resonant characteristic [5]. DGS structures generally affect the filter rejection band but, regarding pass

band filters, the effects of these structures on improving the filter characteristic in pass band are also discussed. Easily fabrication, low insertion loss, and size reduction of the filters are some advantages of using DGS structure in design of filters [6].

For realization of desired DGS structure, considering discussed issues in [6], we utilized simple linear slot in the ground plane of preliminary designed filter. Two simple linear slots are etched in ground plane, one between resonators No. 1 and 2 and the other between resonators No. 3 and 4, in order to improve the mixed coupling of them. Numbering of the resonators can be seen in Fig. 4. The other slots are applied to improve the coupling between the input and output of the filter.

Figure 5. Schematic of designed four-pole SIR filter with DGS.

5. DESIGN AND SIMULATION RESULTS

5.1. Preliminary Four-pole SIR Bandpass Filter

We have used Rogers RT/duroid 6002 substrate with a relative dielectric constant of 2.94, 0.794 mm thickness, and a loss tangent of 0.0012. The designed parameters of resonator of Fig. 1(c) and distance between the resonators of Fig. 4 are summarized in Table 1.

One of the important parameters of the design is the distance between the middle of 50-ohm exciting line and the middle of the

Table 1. Designed parameters of the filter.

L_1	L_2	W_1	W_2	W_a	d	d_{14}	d_{23}	$d_{12} = d_{34}$
4.26 mm	4.37 mm	2.7 mm	2.06 mm	0.5 mm	12.63 mm	0.89 mm	0.77 mm	2.65 mm

Figure 6. Simulation of prelimi-
nary designed four-pole SIR filter
without DGS.
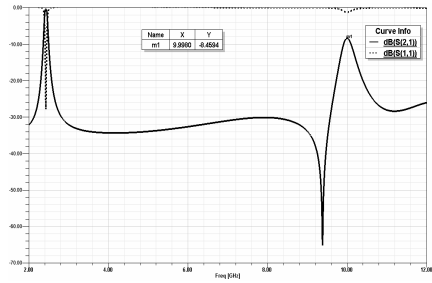
Figure 7. Simulation of rejection
band of the SIR filter without
DGS.

resonator air gap. Considering design limitations, we have selected
smaller value for this parameter in order to weaken the coupling
of input and output and increase the quality factor. Here, this
parameter has been selected as 0.92 mm. The width of exciting strip
line was determined according to the 50-ohm matching impedance. We
adjusted the value of 1 mm for this parameter.

The whole simulations are performed by Ansoft HFSS 11. The
results of preliminary designed four-pole SIR filter simulation in
Section 3 are seen in Fig. 6.

We can observe bandpass filter behavior with central frequency of
2.42 GHz, and bandwidth of 75 MHz in Fig. 6. The insertion loss is
also 0.5 dB and return loss is better than 27 dB.

We expect a wide rejection band of the filter due to using resonator
type of Fig. 1(c) in designed filter. Fig. 7 shows the results of simulation
of the mentioned filter in the frequency range 2–12 GHz.

As can be seen in Fig. 7, the difference between the fundamental
resonant frequency (2.4 GHz) and the first spurious resonant frequency
(10 GHz) is about 7 GHz.

5.2. Four-pole SIR Pass Band Filter with DGS

In order to eliminate the spurious response of the filter in rejection
band and improve insertion loss and return loss in pass band, we
employed DGS mentioned in Section 4. The position of these slots is
determined and optimized according to simulation of surface currents
on the resonators.

Dimensions of used DGS slots in Fig. 5 are identified in the
Table 2, where row (a) denotes dimensions of the slots placed between
resonators 1–2 and 3–4, row (b) for the slots 1–4 and, row (c) for the

slots placed at input and output of the filter, respectively.

Figure 8 shows the result of simulation of passband of the four-pole SIR filter with DGS.

As observed in Fig. 8, insertion loss is 0.55 dB and return loss is better than 14 dB. The bandwidth of the filter reached to 90 MHz at the 2.4 GHz central frequency which is 15 MHz wider than earlier.

We can see 8.6 dB improvements in insertion loss of the first spurious resonant frequency of the filter according to Fig. 9. In fact,

Table 2. Summary of dimensions of DGS slots.

DGS	DGS Length (mm)	DGS Width (mm)
(a)	6.13	0.48
(b)	4.7	1.79
(c)	3.96	1
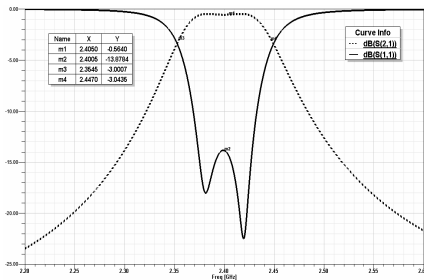
Figure 8. Simulation of pass band of the improved four-pole SIR filter with DGS.
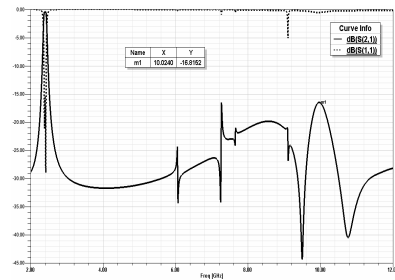
Figure 9. Simulation of the SIR filter with DGS in the range 2–12 GHz.
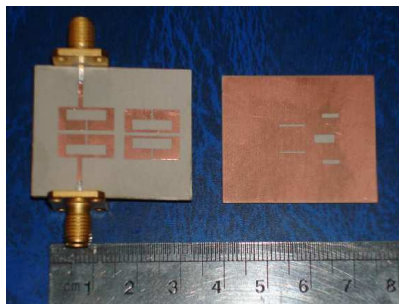
Figure 10. Photograph of the fabricated four-pole SIR bandpass filter with DGS.

insertion loss at frequency 10 GHz reaches to 16.8 dB. In addition, comparing the frequency response of the preliminary SIR filter (without DGS) to the SIR filter with DGS in Fig. 7, we observe elimination of the spurious frequency response in frequency 10 GHz.

5.3. Measured Results and Comparing Them with Simulated

A sample of four-pole SIR bandpass filter with DGS was fabricated and measured. The sample was constructed using Rogers RT/duroid 6002 substrate with relative dielectric constant of 2.94, 0.794 mm thickness, and loss tangent of 0.0012. Photograph of the fabricated filter with DGS is shown in Fig. 10. The prototype circuit size of the filter is around 36 mm × 26 mm.

Measurement was carried out using an Agilent Hp 8720B Network Analyzer. The results of S-parameter in pass band for fabricated
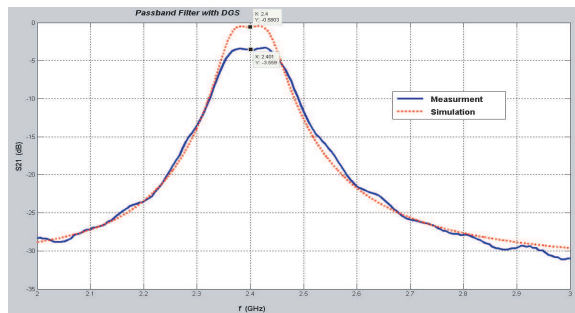
(a)
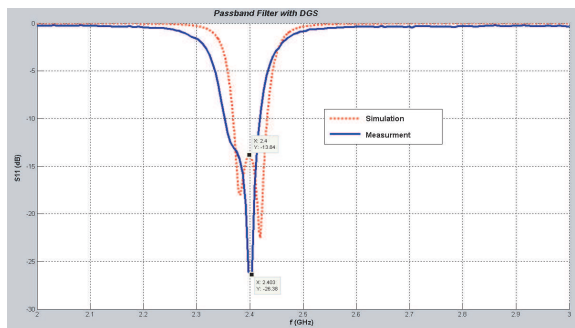
(b)

Figure 11. (a) Measured and simulated results of S_{21} response in pass band. (b) Measured and simulated results of S_{11} response in pass band.
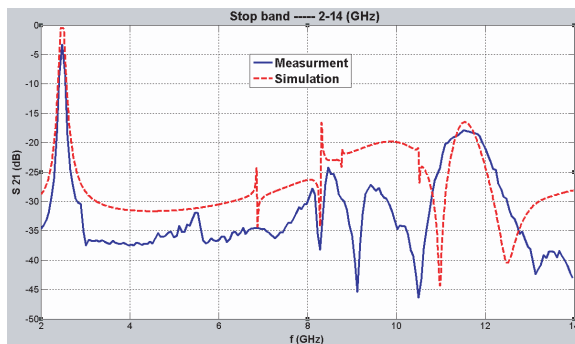
Figure 12. Measured and simulated results of S_{21} response in rejection bandwidth.

sample compared to simulated results are shown in Fig. 11. As it is observed in Fig. 11(a), insertion loss of fabricated model is $-3.56\,\text{dB}$ in center frequency, which is about $3\,\text{dB}$ more than simulation. In addition, return loss of fabricated model is $-26.38\,\text{dB}$, which is improved as $12.5\,\text{dB}$ compared with simulation, as seen in Fig. 11(b).

The measured sample presented a good response in rejection band, as illustrated in Fig. 12. Results of simulation are also shown in Fig. 12 in order to compare. According to Figs. 11(a) and (b), insertion loss in measurement is lower and return loss is higher than simulation.

6. CONCLUSION

In this paper, we have designed and fabricated a four-pole cross-coupled SIR filter. By etching simple linear slots in the ground plane, we have obtained a great improvement in the first spurious resonant frequency elimination. The measured results in the pass band and rejection band are in a good agreement with the simulated ones.

REFERENCES

1. Hong, J. S. and M. J. Lancaster, *Microstrip Filters for RF/Microwave Applications*, John Wiley & Sons, 2001.
2. Hong, J. S. and M. J. Lancaster, "Theory and experiment of novel microstrip slow-wave open-loop resonator filters," *IEEE Transactions on Microwave Theory and Techniques*, Vol. 45, No. 12, December 1997.

3. Makimoto, M., S. Yamashita, and M. Sagawa, "Geometrical structures and fundamental characteristics of microwave stepped-impedance resonators," *IEEE Transactions on Microwave Theory and Techniques*, Vol. 45, No. 7, July 1997.

4. Hong, J. S. and M. J. Lancaster, "End-coupled microstrip slow-wave resonator filter," *Electron. Letters*, Vol. 32, 1494–1496, 1996.

5. Abdel-Rahman, A., A. K. Verma, A. Boutejdar, and A. S. Omar, "Compact stub type microstrip band pass filter using defected ground plane," *IEEE Microwave and Wireless Components Letters*, Vol. 14, No. 4, April 2004.

6. Ahn, D., et al., "A design of the low-pass filter using the novel microstrip defected ground structure," *IEEE Transactions on Microwave Theory and Techniques*, Vol. 49, No. 1, January 2001.